Research Square

Preprints are preliminary reports that have not undergone peer review.
They should not be considered conclusive, used to inform clinical practice,
or referenced by the media as validated information.

Process design and enhancement of extraction distillation for separating n-propanol and dimethyl carbonate using imidazolium-based ionic liquids

Xin Wang
Weifang University of Science and Technology
Xiaokun Wang
Weifang University of Science and Technology
Han Liu
Weifang University of Science and Technology
Chao Sun
kdsunchao@163.com

Weifang University of Science and Technology

Research Article

Keywords: Ionic liquids, Extraction distillation, Multi-objective optimization, Heat integration

Posted Date: June 30th, 2026

DOI: https://doi.org/10.21203/rs.3.rs-10074751/v1

License: This work is licensed under a Creative Commons Attribution 4.0 International License.
Read Full License

Process design and enhancement of extraction distillation for separating n-propanol and dimethyl carbonate using imidazolium-based ionic liquids

Xin Wang[a], Xiaokun Wang[a], Han Liu[a], Chao Sun [a]*

[a] *Shandong Peninsula Engineering Research Center of Comprehensive Brine Utilization, Weifang University of Science and Technology, Weifang 262700, China*

***Corresponding Author**

Chao Sun

Shandong Peninsula Engineering Research Center of Comprehensive Brine Utilization, Weifang University of Science and Technology, Weifang 262700, China

*E-mail: sunc10517@wfust.edu.cn

Abstract

Extractive distillation (ED) ranks among the most potent methods when it comes to resolving azeotropic separation challenges, and the performance of the extractant is the core factor affecting process efficiency. This study centers on the challenges associated with the separation of the DMC-NPA azeotropic mixture. Initially, by virtue of COSMO theory and quantum chemical principles, [EMim][AC] was identified as the optimal extractant from a pool of 40 imidazolium-based ionic liquids (ILs). Then, molecular dynamics simulation techniques were employed to unravel the intrinsic extraction mechanism of the extractant. Finally, the separation design was simulated via Aspen V14 with [EMim][AC] as the extractant, and the results of multi-objective optimization (MOO) showed the [EMim][AC]-ED system demonstrates inferior TAC and diminished gas emissions when contrasted with the DMSO-HIED process. In addition, heat integration was performed on the [EMim][AC]-ED process, reducing the TAC to 1.1032 $/Y and Gas emissions to 1420.30 kg/Y, with reductions of 1.77% and 4.58% respectively, proving that [EMim][AC]-HIED was more valuable for application.

Keywords: Ionic liquids; Extraction distillation; Multi-objective optimization; Heat integration

1. Introduction

The limitations of fossil fuels are becoming increasingly evident in modern industry, the research and development of new energy alternatives have become the guarantee of social progress[1, 2]. Currently, lithium-ion batteries, with their immense development potential, occupy the vast majority of the new energy market share[3, 4]. Electrolyte is an important component that affects the performance of lithium batteries, such as Methyl Propyl Carbonate (MPC), dimethyl Carbonate (DMC), and vinyl carbonate (EC), etc. Among them, MPC possesses an ideal dielectric constant and suitable viscosity, which can extend the low-temperature limit of batteries, thereby greatly expanding their application range [5-7], the current reliance of the energy industry on MPC has driven up its demand for production capacity. However, the industrialization of DMC has generated a significant amount of industrial waste liquids containing DMC and NPA, and the presence of azeotropic systems has exacerbated the difficulty of post-treatment[8]. Enhancing production capacity while increasing the recycling of materials is the core essence of current green chemistry, so, it is of great significance to explore efficient methods for separating DMC and NPA.

The current mainstream processes for separating azeotropic systems are pressure swing distillation, extractive distillation, and azeotropic distillation[9-11]. Among them, extractive distillation (ED) occupies a dominant position due to its excellent separation efficiency and low energy consumption, which has been verified in numerous studies[12-14]. The decisive factor in the ED process is the extractant, whose performance directly affects the extraction efficiency. Moreover, its

development is advancing rapidly, especially with the emergence of efficient green solvents such as ionic liquids (ILs), which have greatly propelled the development of the extraction distillation industry[15-17]. Blahut et al.[18] studied the extraction distillation separation process of DMC and methanol, compared the extraction capabilities of various imidazolium-based ionic liquids, and ultimately selected [EMim][TCB] as the agent, The results showed that this ED process had significant extraction effects and great industrial prospects. Zhu et al.[19] evaluated the separation capacity of four imidazolium-ILs for the EAC-ethanol azeotropic system, and the experimental results verified the remarkable separation capability of the employed ILs. Yan et al.[20] probed the extraction mechanism of different ILs in MeOH and ethyl acetate systems, ultimately selecting [EMim][DEP] as the extractant. Subsequently, Aspen software was employed for the simulation of the process, with the outcomes indicating that its extraction performance was superior to that of the DMSO extraction process. ILs with excellent extraction performance have shown a trend of gradually replacing conventional solvents, which is basically in compliance with the underlying mechanisms of contemporary green development.

The simulation design of processes is a prerequisite for industrialization, with the deepening of economic transformation, qualified process design must take into account both environmental impacts and economic cost. Multi-objective optimization (MOO) is an integrated optimization approach for processes, targeting both operational costs and gas emissions, and has been applied in numerous studies [21-23]. Zhong et al. [24] designed various extraction distillation processes to separate water,

EtOH, and Ethyl tert-butyl ether, after MOO of the process, the optimal separation process was obtained. Shan et al. [25] designed an extraction distillation separation process for toluene-methanol-water, and optimized the process with production cost and gas emissions as the objectives, resulting in a scheme that achieves a comprehensive balance between cost and environmental impact. As consequence, the MOO design of the separation process can reduce environmental impact while also lowering costs, which is an effective measure to obtain the best solution.

This study endeavors to reveal the extraction mechanism of ionic liquids in the separation process, and design and optimize a process scheme that balances economic efficiency and environmental performance, providing a basis for the green and efficient separation of DMC and NPA. Firstly, three ILs ([EMim][DEP], [EMim][H_2PO_4], and [EMim][AC]) were preliminarily acquired according to the COSMO theory[26], then, the mutual penetration distance was calculated using the Multiwfn 3.8 to quantify the strength of interaction and compare extraction capabilities[27]. Simultaneously, the mechanism of each IL was intensively probed utilizing molecular dynamics (MD) simulation. Thereafter, combined with the multi-objective optimization (MOO) method, the process was simulated via Aspen Plus, and further enhanced through thermal integration, ultimately leading to the acquisition of the optimal separation scheme. This research provides molecular-level insights into the extraction mechanism of ILs, while proposing a high-efficiency and feasible strategy for realizing the effective separation of NPA and DMC.

2 Methodology for extractant screening

2.1 COSMO model

Due to the designability inherent in ILs, significant disparities exist in their performance, while their extraction capacities also show notable differences among various systems. So, efficient screening has always been a research hotspot. In current numerous studies[28-30], COSMO-RS theory has emerged as the most sophisticated approach for tackling relevant problems, the core of this theory lies in gaining chemical potential via statistical thermodynamic calculations, thereby enabling the prediction of the related properties[26]. In this work, the infinite activity coefficients (γ^{∞}) were calculated through COSMOthermX (v22.0.0), and the selectivity coefficients (S^{∞}) were obtained by the following formulas.

$$S^{\infty}_{NPA,\ DMC} = \frac{\gamma^{\infty}_{DMC,IL}}{\gamma^{\infty}_{NPA,IL}} \tag{1}$$

Where the $\gamma^{\infty}_{NPA,IL}$ and $\gamma^{\infty}_{DMC,IL}$ are the activity coefficients of NPA, and DMC in the corresponding IL, respectively. The S^{∞} is positively proportional to the extraction performance [31].

2.2 QC calculations

Quantum chemical (QC) calculation is an effective strategy for quantifying the strength of intermolecular interactions, which can further serve as a basis for screening extractants[32, 33]. Generally, QC calculations are based on the optimal molecular composite structure. In this part, the initial structures of the ILs, NPA, and DMC were retrieved from the corresponding database, and then optimized for structure and energy using Gaussian software[34]. The specific steps for the operation are summarized in Section 1 (Supplementary Material). On the basis of the optimized

structures, ESP (electrostatic potential) and MPD (mutual penetration distance) analyses were carried out utilizing Multiwfn 3.8 and VMD [26, 35].

3 Mechanism exploration method

Molecular dynamics (MD) simulation is a method based on electrostatic Newtonian mechanics, which predicts the thermodynamic properties of particles in a system under specific conditions by simulating their changes over time[36]. In this work, the topology files essential for the simulation were constructed using the Sobtop program[37], MD simulations of the DMC-NPA-IL system were carried out using GROMACS 2022.3[38, 39]. The simulation steps are summarized within Section 2 (Supplementary Material). According to the simulation results, further comparative analysis were performed from the aspects of interaction energy and spatial distribution function (SDF) by virtue of the Travis and VMD[40].

4 Process analysis methods

With [EMim][AC] employed as the extractant, the ED process for this system was modeled via Aspen Plus, and multi-objective optimization and process enhancement were carried out sequentially.

4.1 Economic analysis

In industrial design, the operational cost of the process and the capital cost of equipment are the core components for measuring the economic performance of the process. Therefore, in economic evaluation, the total annual cost (TAC) of process operation is divided into the total capital cost (TCC) and the total operating cost (TOC) [41], which can be computed by virtue of the following formula:

$$TAC = TOC + \frac{TCC}{payback\ period} \tag{2}$$

Normally, the TOC mainly consist of the expenses associated with electricity usage, condensed water consumption, and heating steam demand [42, 43], while the TCC comprises the capital investment for tower shell and internals, as well as heat exchangers, and the payback period for those equipment is 3 years, it is worth mentioning that some accessories such as pipelines, and reflux tanks are not included in the investment costs. The calculation parameters and formulas are presented in Table S1(Supplementary Material).

4.2 Environmental analysis

The emission of polluting gases is an important factor in the decline of environmental indices, and reducing their emissions is one of the approved goals pursued in process design. In this study, gas emissions were considered as one of the optimization objectives. The heat source of the distillation tower comes from high-pressure steam from the thermal power plants, and the heat source of the steam depends on the combustion of coal, which produces a large amount of harmful gases (CO_2, SO_2 and NO_X) [44]. Reasonable regulation of steam usage can effectively reduce energy consumption, which further decreases gas emissions and ultimately attains the goal of environmental conservation.

5 Results and Discussion

5.1 Extractant selection analysis

5.1.1 Selectivity analysis

The selectivity coefficients (S^{∞}) of the ILs and the organic solvents are listed in

Fig.1, and the relevant numerical results are tabulated in Table S2 (Supplementary Material).

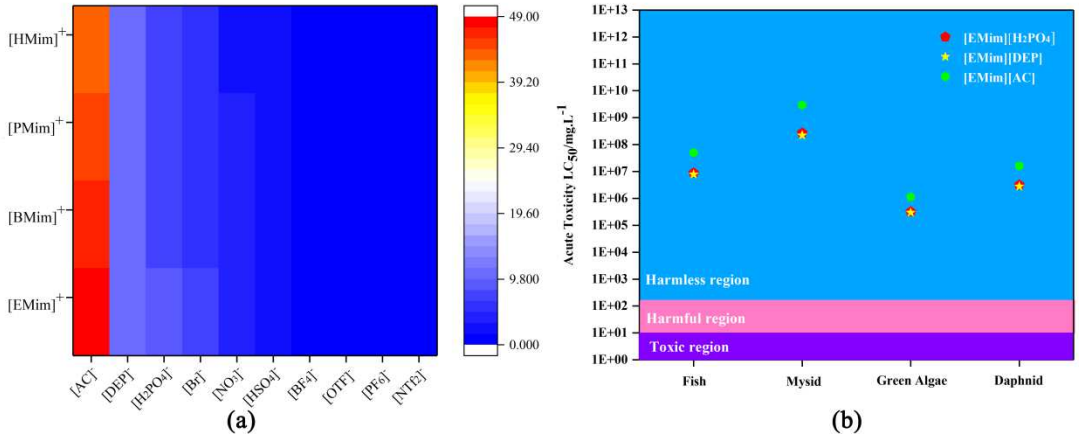


Fig. 1. The selectivity of the selected extractants

As illustrated in Fig.1(a), the separation selectivity of different ILs for the DMC-NPA system varies significantly. In particular, the acetate-based ILs exhibit extremely remarkable separation selectivity, among them, the selectivity of [EMim][AC] is 48.8879, which is the most significant. The extraction selectivity of diethyl phosphate-based ILs and dihydrogen phosphateis-based ILs also own excellent extraction performance. Additionally, the shorter the branch of the cation in the IL, the lower its viscosity and the more thorough the mass transfer. As a result, [EMim][AC], [EMim][DEP] and [EMim][H_2PO_4] were initially designated as the potential extraction agents for the next step of analysis.

Furthermore, environmental assessment indicators of the three ILs were analyzed and calculated based on the ECOSA model [45], as illustrated in Fig.1, and relevant numerical results are summarized in Table S3 (Supplementary Material), as revealed by the toxicity data, there are slight differences in the environmental toxicity of the chosen ILs. Notably, [EMim][AC] possesses the lowest toxicity among the

candidates, followed by [EMim][H_2PO_4] and [EMim][DEP], nevertheless, all candidates are located in the non-toxic zone. Accordingly, these three ILs are feasible for extracting NPA from DMC.

5.1.2 ESP analysis

ESP distribution enables the intuitive visualization of molecular surface charge characteristics, allowing for the identification of reaction active sites and intermolecular interaction modes[46]. Electrostatic attraction is the essence of intermolecular hydrogen bonding formation[47, 48], the electrostatic attraction formed at the extremum point is the greatest, and the structure possesses optimal stability[49], the stability of the structure is also an effective method to measure the extraction ability of the extractant.

In the present research, ESP parameters corresponding to NPA, DMC, and the ILs were calculated sequentially using Multiwfn, which are illustrated in Fig.2 and Fig.S1.

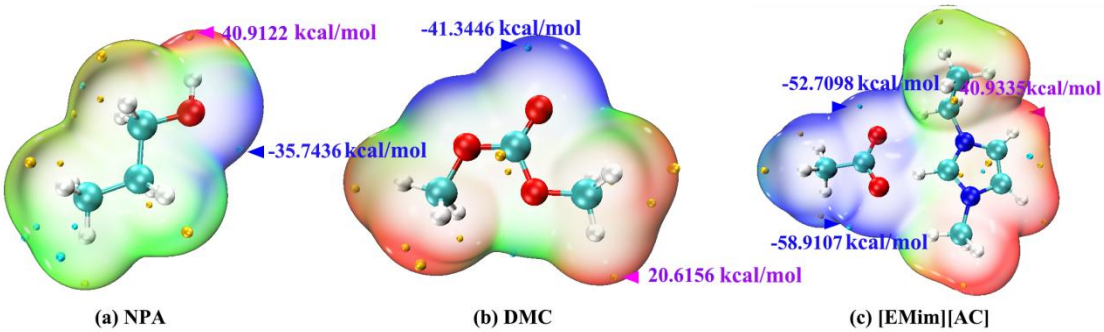


Fig. 2 ESP on vdW surfaces of all substance

Fig.2 clearly demonstrates the distribution of extreme points of molecular surface electrostatic potential, the blue sphere located in the blue region denotes the minimum value point of the corresponding segment, whereas the yellow sphere in the

red region stands for the maximum value point within the section. As presented in Fig.2(a), the minimum value on the surface of NPA is -35.7436 kcal/mol, while the maximum value point near H is 40.9122 kcal/mol, and these two points have great potential for forming hydrogen bonds. Likewise, As displayed in Fig.2(c), the maximum point of the electrostatic potential on the surface of [EMim][AC] is 40.9335 kcal/mol, and the minimum point is -58.9017 kcal/mol. When [EMim][AC] is added to the system, due to the electrostatic complementarity effect, the optimal reaction sites are located on the H of NPA and the O of [EMim][AC], thereby forming a stable hydrogen bond. Owing to the hydrogen-bonding effect, [EMim][AC] can associate with NPA to construct a stable composite structure. Moreover, greater structural stability corresponds to stronger extraction capability and more effective azeotrope breaking. Following the identical theoretical principles, the optimized stable configurations of the IL-NPA/DMC were determined, which are illustrated in Fig.S2.

5.1.3 Mutual penetration distance (MPD) analysis

The penetration of the molecular vdW surface[46] is triggered by electrostatic interactions, and the distance is directly proportional to the strength of the interaction [50]. By quantifying the penetration distance of the van der Waals surface, the strength of hydrogen bonding can be relatively accurately compared, thereby providing a basis for the comparison of extraction capabilities. In this part, the penetration distance between NPA/DMC and different ILs were calculated by Multiwfn, and depicted in Fig.3. Fig.3 showed that the red region corresponds to the

electron-deficient area, and the green region denotes the electron-rich area. The overlapping area between them is caused by their mutual penetration, demonstrating a certain intensity of electrostatic attraction. A large penetration distance corresponds to a strong hydrogen bond interaction, and also indicates excellent extraction capacity.

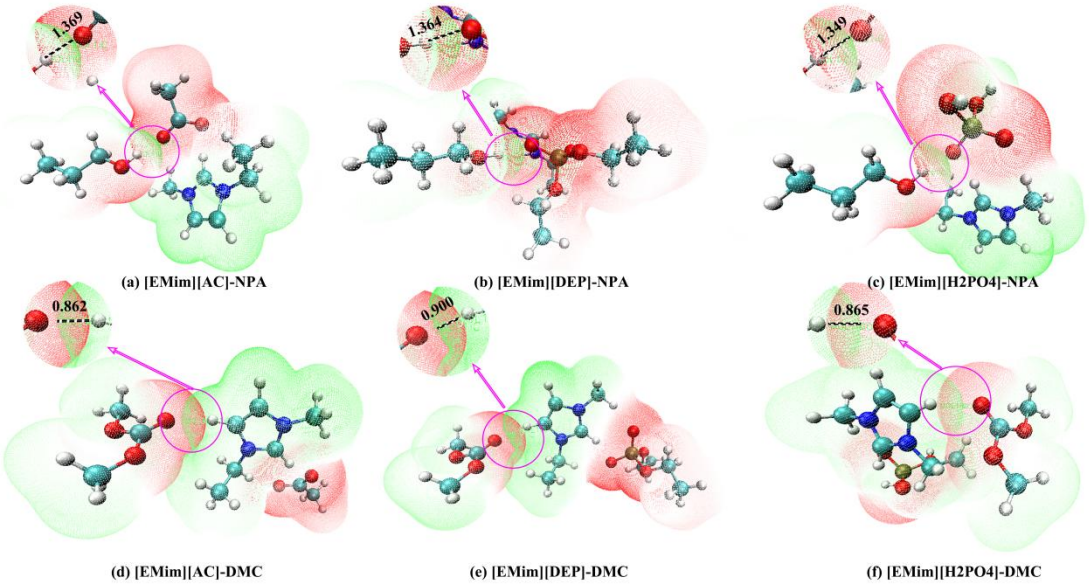


Fig.3 Mutual penetration distance of different IL-NPA/DMC

As can be seen in Fig.3(a), the MPD between [EMim][AC] and NPA is 1.369 Å, which is much greater than that between [EMim][AC] and DMC (0.862 Å). This reveals that the intermolecular interaction between [EMim][AC] and NPA is considerably stronger than that between [EMim][AC] and DMC. Throughout the extraction procedure, the [EMim][AC]-NPA complex exhibits higher structural stability, which facilitates the separation of DMC from the upper part of the distillation column. Likewise, [EMim][DEP] and [EMim][H_2PO_4] both exhibit stronger affinity toward NPA relative to DMC, which manifests that the two ILs are also feasible for extractive distillation separation in the DMC-NPA system. Additionally, [EMim][AC] exhibits a longer MPD toward NPA in contrast to

[EMim][DEP] and [EMim][H_2PO_4], which indicates that [EMim][AC] possesses the optimal extraction performance. Further comparison on their penetration distances demonstrates the ranking of their extraction capacities as follows: [EMim][AC]>[EMim][DEP]> [EMim][H_2PO_4].

5.2 MD analysis

5.2.1 Spatial distribution function(SDF) analysis

Investigating the microscopic mechanism of extractive separation is crucial for comprehensively analyzing the extraction process. SDF analysis serves as a crucial analytical tool in molecular dynamics studies, as it illustrates the movement principles by depicting the distribution variations of target ions within a specific region around the central particle.

In this study, SDF profiles of relevant reference atoms were constructed via GROMACS 2020.3 and TRAVIS, and visual rendering was realized by means of VMD. All corresponding diagrams are illustrated in Fig. 4.

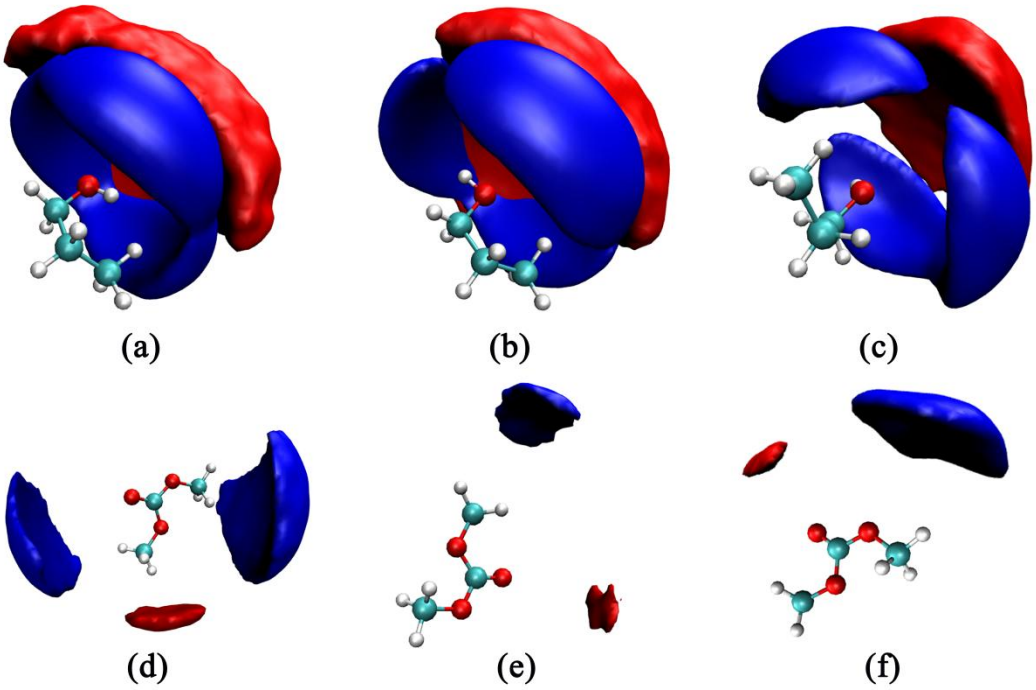


Fig.4 SDF between IL and NPA/DMC (rad represents SDFs of $[EMim]^+$ (islvalue=4.8), blue represents the different anions(isovalue= 3.5), (a) $[EMim]^+$ and $[AC]^-$ around NPA, (b) $[EMim]^+$ and $[DEP]^-$ around NPA, (c) $[EMim]^+$ and $[H_2PO_4]^-$ around NPA, (d) $[EMim]^+$ and $[AC]^-$ around DMC, (e) $[EMim]^+$ and $[DEP]^-$ around DMC, (f) $[EMim]^+$ and $[H_2PO_4]^-$ around DMC)

In Fig.4(a), the blue isosurface represents $[AC]^-$, while the red isosurface corresponds to the $[EMim]^+$, the density distribution of $[AC]^-$ is concentrated in the region adjacent to NPA, demonstrating that the anion preferentially interacts and binds with NPA during the combination process. Furthermore, the size of the isosurface is proportional to the distribution of density. By comparing Fig.(a) and (d), it can be observed that he density distribution of [EMim][AC] around NPA is more concentrated than that around DMC, demonstrating that [EMim][AC] has a stronger affinity for NPA, enabling the extraction and separation of the system. For the other two ILs, the density distribution is similar, so the extraction and separation of the system can also be achieved. In addition, as depicted in Fig.4(b), [EMim][DEP]

presents a looser density distribution around NPA in contrast to [EMim][AC], which indicates that [EMim][DEP] interacts with NPA with weaker strength in comparison to [EMim][AC], the main cause of this difference lies in the difference in electronegativity of O on different anions. Similarly, the density distribution of [EMim][H_2PO_4] around NPA is minimal as presented in Fig.4(c), corresponding to its relatively weak extraction performance. The result is in agreement with the result obtained from QC calculations.

5.2.2 Non-bonding interaction energy analysis

As an important notion in molecular dynamics research, non-bonding interaction energy is utilized to quantify the intensity of intermolecular forces, and can be used to explore the impact of structural differences on performance. non-bonding interactions have two main manifestations: electrostatic Coulombic force and van der Waals force. electrostatic interactions and vdW interaction. In this part, the interaction energies of each IL with NPA and DMC are demonstrated in Fig.5 and Table S4 (Supplementary Material).

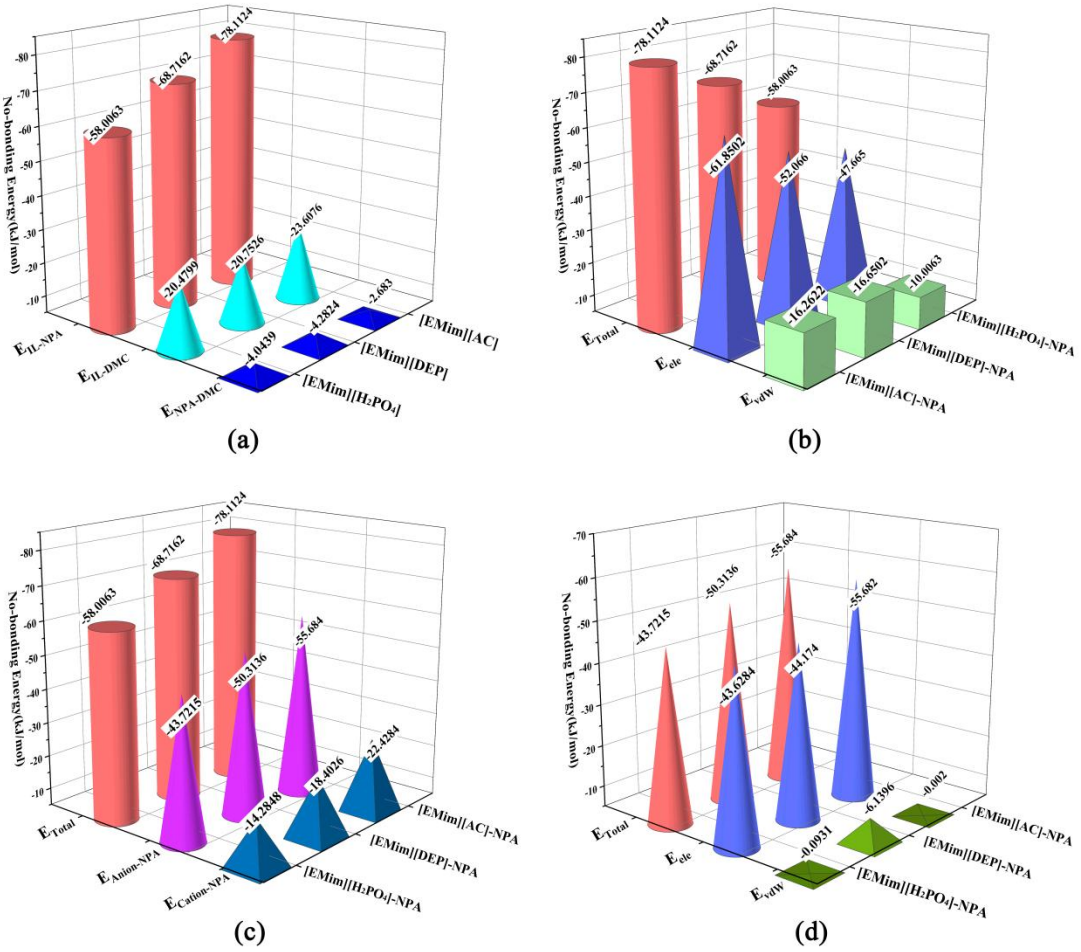


Fig. 5 Non-bonding interaction energy of DMC-NPA-IL

Fig.5(a) demonstrates that the energy between [EMim][AC] and NPA is -78.1124 kJ/moL, which far exceeds the total non bonding interaction energy between [EMim][AC] and DMC(-23.6076 kJ/moL), as well as the interaction energy between DMC and NPA (-2.6830 kJ/moL). That is to say, [EMim][AC] can effectively break the bonding between DMC and NPA, forming a new and more stable composite structure, thereby achieving the effect of extraction and separation. Although all the selected ionic liquids can achieve this purpose, from the viewpoint of the interaction energy values, it is obvious that [EMim][AC] exhibits more favorable extraction efficiency compared with [EMim][DEP] and [EMim][H_2PO_4]. In addition, as

presented in Fig.5(b), for the intermolecular binding between [EMim][AC] and NPA, the electrostatic contribution is -61.8502 kJ/moL, which accounts for 79.18% of the total interaction energy, similarly, electrostatic energy contributes 75.77% to [EMim][DEP]-NPA interaction and 82.17% to [EMim][H_2PO_4]-NPA interaction, indicating that the electrostatic force of ILs is dominant. Meantime, as depicted in Fig.5(c), the energy between anion and NPA is much greater than that between cation and NPA, revealing that the anion of the IL play the main role during the process, while the cation play a supporting role. Precisely speaking, as shown in Fig.5(d), the electrostatic interaction of the anions is dominant, and the van der Waals force is auxiliary, this discovery will provide a basis for our later design of ILs.

5.3 Process design and optimization

This study utilized Aspen Plus V14 software to simulate the ED process of the NPA-DMC system, where [EMim][AC] served as the extractant. During the optimization process, eight variables including tray number, extractant feed rate, and feed plate position were investigated with total annual cost (TAC) and gas emission as the dual objective functions, and the iteration was terminated once the calculation results remain unchanged. The MOO process is listed in Fig.S3.

5.3.1 Design and Optimization of [EMim][AC]-ED Process

In this study, the feeding rate of the raw material stream was maintained at 100 kmoL/h, wherein the molar ratios of DMC to NPA were 0.634 and 0.366, correspondingly. [EMim][AC] were defined by means of the UNIFAC-Lei model [51-55], the essential parameters, such as volume parameters (R_k), surface area

parameters (Q_k) , and the binary interaction parameters of relevant functional groups are listed in Table S5, and S6, the scalar parameters of [EMim][AC] [56] are presented in Table S7. The corresponding optimum results are illustrated in Fig.6.

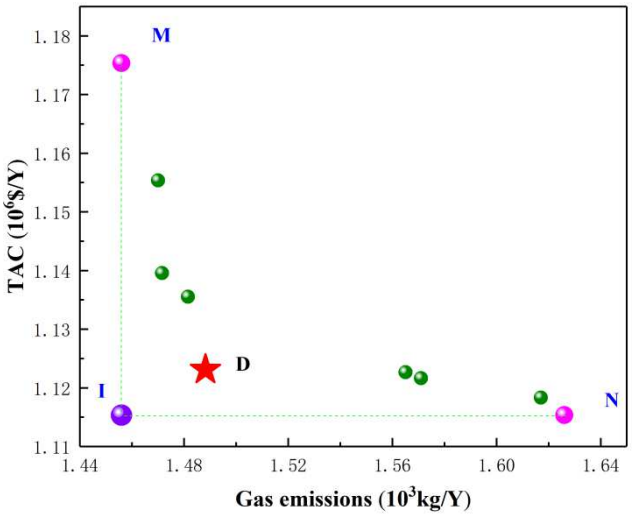


Fig.6 TAC and Gas emissions for [EMim][AC]-ED scheme

According to Fig.6, point M corresponds to the process featuring minimal gas emissions(about 1457kg/Y), however, its TAC reaches approximately 1.175×10^6 \$/Y, while point N corresponds to the scheme possessing the lowest TAC (about 1.115×10^6 \$/Y) and a high Gas emissions (about 1623 kg/Y). Apparently, no direct proportional relationship is observed between TAC and Gas emission, the two objectives can not reach their respective minima at the same time. Therefore, Point I is difficult to achieve. Accordingly, through overall evaluation, point D adjacent to ideal point I is selected as the optimum scheme, and the detailed optimal operating parameters are tabulated in Table S8, and the [EMim][AC]-ED process is illustrated in Fig.7.

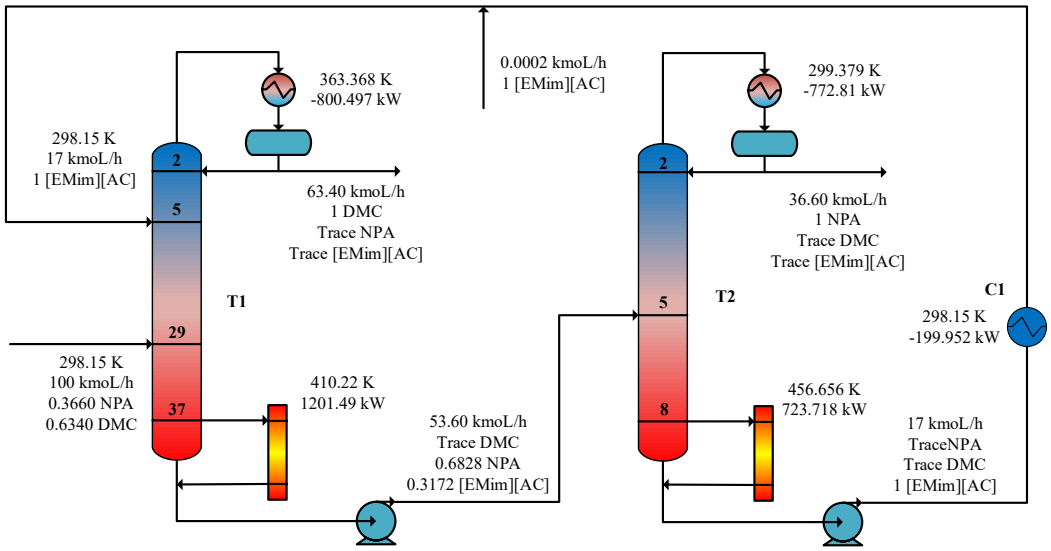


Fig.7 The [EMim][AC]-ED process

As illustrated in Fig. 7, [EMim][AC] and the raw mixture were fed into column T1 at the 5th and 29th theoretical plate, respectively. The optimal feeding rate of [EMim][AC] was 17 kmoL/h, DMC product with a purity of 1 can be collected at the tower top, while the bottom stream of T1 passed through 5th stage and entered T2. Then, High-purity NPA (mole fraction= 1) was recovered from the overhead of T2 at a flow rate of 36.60 kmoL/h, while the [EMim][AC] with a mole fraction of 1 was extracted from the bottom of the tower at a flow rate of 17 kmoL/h. Finally, [EMim][AC] was cooled to 298.15 K by the condenser C1 and then recycled to T1 for reuse.

5.3.2 [EMim][AC]-HIED process

Thermal integration is an important means to reduce the energy consumption in the distillation process. In the distillation separation process described above, the bottom effluent from the solvent recovery tower T2 carried abundant thermal energy. Direct cooling via condenser C1 would lead to unnecessary heat loss and excessive

consumption of cooling water. Therefore, it is necessary to make reasonable and effective use of this part of the heat. In this part, the T-H (Temperature-Enthalpy) diagram for the ED process is depicted in Fig.S4.

Fig.S4 demonstrates that the dark green region denotes the area available for heat recovery, and the amount of energy is 87.96 kW. A considerable temperature gradient exists between the bottom streams of solvent recovery tower T2 and tower T1. Accordingly, the residual heat of the high-temperature [EMim][AC] extracted from T2 is utilized to assist in heating the bottom of the T1, thereby cutting down the steam demand of T1 and cooling water usage of C1. The HIED process is tabulated in Fig.8.

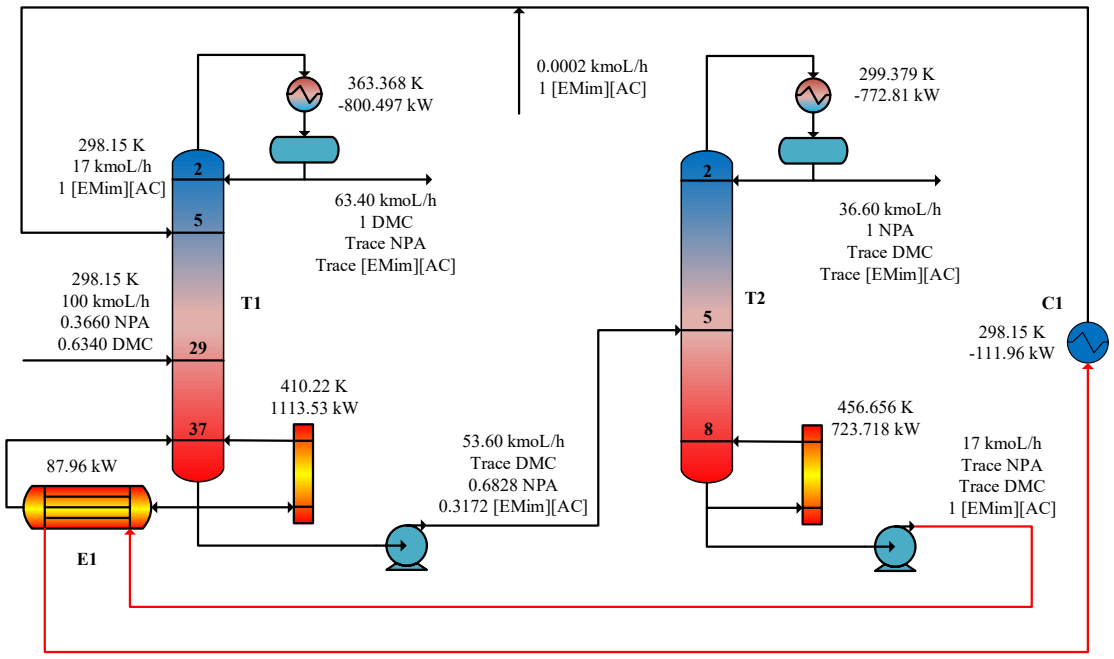


Fig.8 Heat integrated ED process

5.3.5 Economic analysis

The economic efficiency of the process is the primary consideration in the design process, and serves as the direct evaluation criterion for the feasibility of the process. In this work, the investment costs and operating costs of each equipment in the

process have been computed and tabulated in Table S9, the cost are presented in Fig.9.

As demonstrated in Fig.9, the TAC of the [EMim][AC]-ED process is 1.1231×10^6 \$/Y, and the TAC of the [EMim][AC]-HIED drops to 1.1032×10^6 \$/Y after heat integration, which is a approximately 1.77% reduction compared to the [EMim][AC]-ED process, and the reduction mainly occurs in the TOC. Compared with the extractive distillation process adopting DMSO as the extractive solvent [57], the TAC of [EMim][AC]-HIED is 55.04% lower than the TAC of the DMSO-HIED process (2.4535×10^6 \$/Y), indicating that [EMim][AC] has superior extraction performance compared to the traditional organic solvents. Consequently, from the perspective of economic benefits, the [EMim][AC]-HIED process is a more suitable scheme.

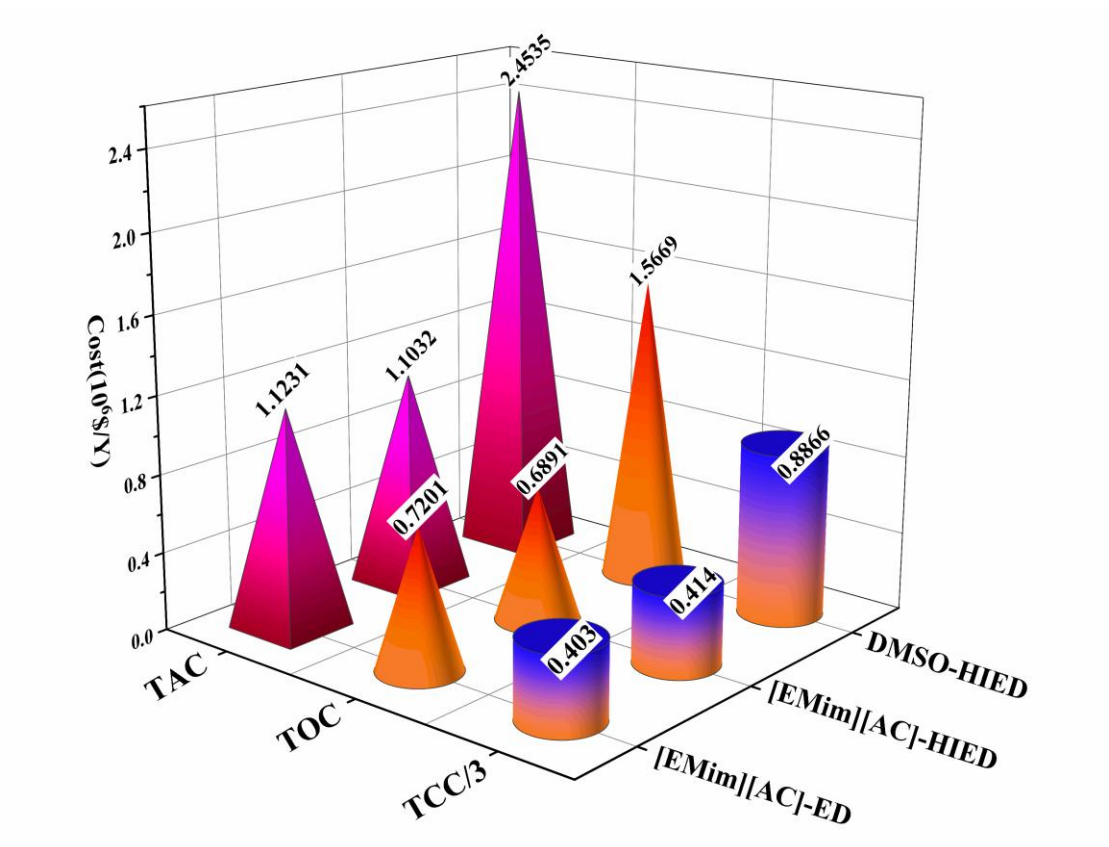


Fig.9 The cost of the simulated schemes

5.3.6 Environmental analysis

Against the backdrop of national dual-carbon goals, environmental friendliness serves as another crucial design criterion for chemical processes. In chemical processes, the emission of polluting gases represents the primary environmental impact. In this part, the polluting gases such as CO_2, SO_2, and NO*x* were calculated and depicted in Fig.10, and the values are tabulated in the Table S10.

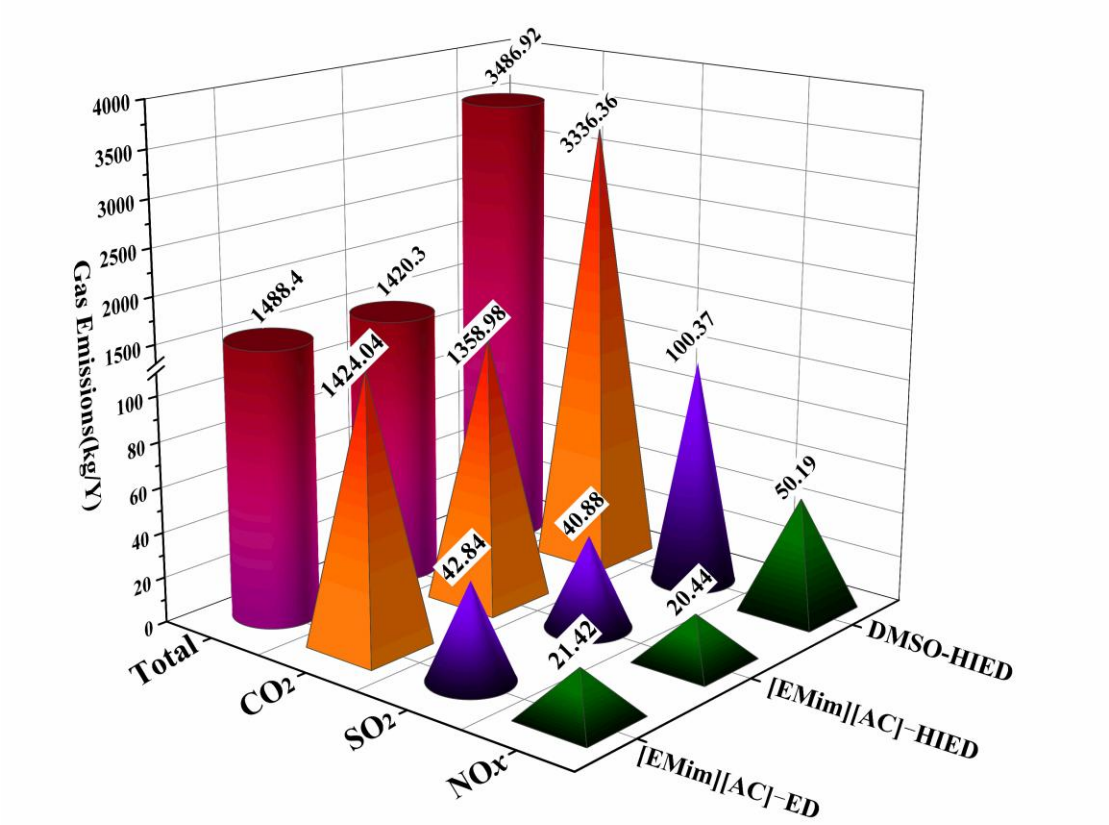


Fig.10 Gas emissions of the simulated schemes

As demonstrated in Fig.10, the total gas emissions of the [EMim][AC]-ED process are 1488.4 kg/Y, while those of the [EMim][AC]-HIED process are 1420.3 kg/Y, representing a reduction of 4.58% compared with the [EMim][AC]-ED process. Additionally, in our previous research[57], the total gas emissions of the DMSO-HIED process are 3486.92 kg/Y. In comparison, the [EMim][AC]-HIED

process achieves a 59.27% emission reduction, demonstrating remarkable environmental advantages. Accordingly, the [EMim][AC]-HIED process is environmentally superior to the traditional solvent-based process.

6 Conclusion

In conclusion, the NPA-DMC separation process was comprehensively explored by means of mechanism analysis and process simulation. Through the combination of COSMO model and QC analysis, comparative evaluations were conducted, leading to the selection of [EMim][AC] as the preferred extractant for the NPA-DMC system. Additionally, the extraction mechanism of the extractant in the system was explored, notably, the anion of IL exerts a predominant effect on the extraction performance, where electrostatic interactions serve as the primary controlling factor. Then, taking [EMim][AC] as the extractant, the ED process was initially designed and optimized, followed by additional process optimization through thermal integration technology, the results showed that the [EMim][AC]-HIED process achieves 1.77% and 4.58% reductions in TAC and gas emissions, respectively, relative to the [EMim][AC]-ED system. Consequently, the [EMim][AC]-HIED process exhibits greater promising application potential in industrial practice.

CRediT authorship contribution statement

Xin Wang: Conceptualization, Methodology, Investigation, Writing-original draft. Xiaokun Wang: Validation, Software. Han Liu: Visualization, Supervision, Software. Chao Sun: Resources, Formal analysis, Writing-review & editing.

Acknowledgements

The Research Start-up Fund Project of Weifang Science and Technology University (Project KJRC2025020), The Key R&D Program of Shandong Province, China(2025CXGC010706)

Nomenclature

[EMim][AC]	1-Ethyl-3-methylimidazolium Acetate
[EMim][DEP]	1-Ethyl-3-methylimidazolium Diethyl Phosphate
[EMim][H_2PO_4]	1-Ethyl-3-methylimidazolium Dihydrogen Phosphate
vdW	van der Waals
ED	Extraction distillation
HIED	Heat integration Extraction distillation

References

[1] X. Zhang, C. Zhao, J. Huang, Q. Zhang, Recent Advances in Energy Chemical Engineering of Next-Generation Lithium Batteries, Engineering. 4 (2018) 632-653. https://doi.org/ 10.1016/j.eng.2018.10.008.

[2] N. Zhang, Y. Lu, S. Kadam, Z. Yu, 2023. Investigation of the integrated fuel cell, battery, and heat pump energy systems. Energy Convers. Manage. 276, 116503. https://doi.org/10.1016/j.enconman.2022.116503.

[3] Y. Feng, L. Zhou, H. Ma, Z. Wu, Q. Zhao, H. Li, K. Zhang, J. Chen, Challenges and advances in wide-temperature rechargeable lithium batteries. Energy Environ. Sci. 15(2022) 1711-1759. https://doi.org/ 10.1039/d1ee03292e.

[4] T. Yang, C. Wang, W. Zhang, Y. Xia, H. Huang, Y. Gan, X. He, X. Xia, J. Zhang, A critical review on composite solid electrolytes for lithium batteries: Design strategies and interface engineering. J. Energy Chem. 84(2023)189-209. https://doi.org/10.1016/j.jechem. 2023.05.011.

[5] C. Su, M. He, P. C. Redfern, L.A. Curtiss, I. A. Shkroba, Z. Zhang, Oxidatively Stable Fluorinated Sulfone Electrolytes for High Voltage High Energy Lithium-ion Battery. Energy

Environ. Sci. 10 (2017) 900-904. https://doi.org/10.1039/C7EE00035A.

[6] S. Uchida, T. Kiyobayashi, 2021. What differentiates the transport properties of lithium electrolyte in ethylene carbonate mixed with diethylcarbonate from those mixed with dimethylcarbonate? J. Power Sources. 511, 230423. https://doi.org/10.1016/j.jpowsour.2021.230423.

[7] Y. Li, Z. Wang, W. Lin, B. Wei, D. Chen, A Concentrated Electrolyte of LiTFSI and Dimethyl Carbonate for High-Voltage Li Batteries. ACS Appl. Energy Mater. 6(2023)9337-9346. https://doi.org/10.1021/acsaem.3c01206.

[8] P. Zhou, 2018. Study on the Separation of Methanol-DMC Azeotropic System by Extractive Distillation with Molecular Simulation. Ningxia University.

[9] J. Cho, J. Jeon, Optimization study on the azeotropic distillation process for isopropyl alcohol dehydration. Korean J. Chem. Eng. 23(2006)1-7. https://doi.org/10.1007/BF02705684.

[10] F. Ganem, S. Mattedi, E. Rodil, A. Soto, Separation of linalool from limonene via extractive distillation with 1-butyl-3-methylimidazolium acetate as entrainer. Ind. Eng. Chem. Res. 59(2020) 19449-19457. https://doi.org/10.1021/acs.iecr.0c03646.

[11] A. Yu, Q. Ye, J. Li, X. Li, Y. Wang, Q. Rui, 2023. Improving the economy and energy efficiency of separating n-propanol/water/tetrahydrofuran via triple-column pressure-swing distillation and azeotropic combining pressure-swing distillation, Sep. Purif. Technol. 309, 123023. https://doi.org/10.1016/j.seppur.2022.123023.

[12] M. Salman, N. Javed, X. Liu, M. He, 2023. Azeotrope separation of ethyl propionate and ethanol by extractive distillation and pressure swing distillation method. Sep. Purif. Technol. 311, 123361. https://doi.org/10.1016/j.seppur.2023.123361.

[13] K. Li, H. Cheng, X. Li, Z. Feng, H. Jin, Z. Li, S. Zheng, 2024. Molecular mechanism-based extractant screening and process design for the separation of methanol/dimethyl carbonate azeotrope, Sep. Purif. Technol. 333, 125916. https://doi.org/10.1016/j.seppur. 2023.125916.

[14] H. Kang, F. Zhao, R. Zhu, Z. Lei, Extractive distillation for separation of isopropanol-n-propanol-water ternary system: Mechanism analysis and process design. Chem. Eng. Res. Des. 200(2023)793-802. https://doi.org/10.1016/j.cherd.2023.11.036.

[15] L. Rebelo, L. Lopes, J. Esperanca, H. Guedes, Accounting for the unique, doubly dual nature of ionic liquids from a molecular thermodynamic and modeling standpoint. Acc. Chem. Res.

40(2007)1114-1121. https://doi.org/10.1021/ar7000556.

[16] W. A. Christinelli, L. G. Trindade, A. B. Trench, C. S. Quintans, C. M. Paranhos, High-performance energy storage of poly (o-methoxyaniline) fifilm using an ionic liquid as electrolyte, Energy, 141 (2017) 1829-1835. https://doi.org/ 10.1016/j.energy.2017.11.026.

[17] Z. Zhu, Y. Xu, H. Li, Y. Shen, D. Meng, P. Cui, Y. Ma, Y. Wang, J. Gao, 2020. Separation of isopropyl alcohol and isopropyl ether with ionic liquids as extractant based on quantum chemical calculation and liquid-liquid equilibrium experiment. Sep. Purif. Technol. 247, 116937.https://doi.org/10.1016/j. seppur. 2020.116937.

[18] A. Blahut, V. Dohnal, Ionic liquid 1-ethyl-3-methylimidazolium tetracyanoborate: An efficient entrainer to separate methanol þ dimethyl carbonate azeotropic mixture. Fluid Phase Equilibr. 423(2016) 120-127.http://dx.doi.org/10.1016/j.fluid.2016.04.021.

[19] Z. Zhu, Y. Ri, H. Jia, X. Li, Y. Wang, Process Evaluation on the Separation of Ethyl acetate and Ethanol using Extractive Distillation with Ionic Liquid. Sep. Purif. Technol. 181(2017) 44-52. http://dx.doi.org/10.1016/j.seppur. 2017.03.011.

[20] L. Yan, J. Li, X. Jian, X. Li, J. Zhang, Q. Ye, Evaluation on the separation effect and extractant recovery efficiency of extractive distillation for separating ethyl acetate/methanol with ionic liquids as extractants. Process Saf. Environ. Prot. 167(2022) 343-355. https://doi.org/10.1016/j.psep.2022.09.010.

[21] Y. Shen, Y. Xu, D. Meng, Z. Chen, H. Li, Y. Zhang, Z. Zhu, J. Gao, Y. Wang, 2021. Molecular mechanism and extraction performance evaluation of ionic liquids for extraction process of n-heptane/n-propanol. Sep. Purif. Technol. 276, 119342. https://doi.org/10.1016/ j.seppur.2021.119342.

[22] H. Zhang, Y. Jiao, Q. Zhao, C. Li, P. Cui, Y. Wang, 2022. Sustainable separation of ternary azeotropic mixtures based on enhanced extractive distillation/pervaporation structure and multi-objective optimization. Sep. Purif. Technol. 298, 121685. https://doi.org/10.1016/j.seppur.2022.121685.

[23] J. Leng, S. Fan, C. Lu, Z. Feng, L. Dong, 2023. Sustainable design and multi-objective optimization of heat pump assisted extractive distillation process for separating a ternary mixture of methyl acetate, tetrahydrofuran and methanol. Journal of Cleaner Production. 419, 138186. https://doi.org/10.1016/j.jclepro.2023.138186.

[24] J. Zhong, H. Cheng, Y. Dai, Y. Jiao, K. Wang, L Xin,, Y. Zhang, Y. Wang, Design and Multiple Performance Evaluation of Green Sustainable Process for Azeotropes Separation via Extractive Distillation. ACS Sustainable Chem. Eng. 11(2023)16849-16881. https://doi.org/10.1021/acssuschemeng.3c05675.

[25] B. Shan, S. Wang, Q. Xu, Y. Wang, P. Cui, F. Zhang, 2024. Design and multi-objective optimization of hybrid extractive distillation process for separating the toluene-methanol-water ternary azeotrope. Sep. Purif. Technol. 336, 126335. https://doi.org/10.1016/j.seppur.2024.126335

[26] E. Mullins, R. Oldland, Y. Liu, S. Wang, S. I. Sandler, C. Chen, K. C. Seavey, Sigma-Profile Database for Using COSMO-Based Thermodynamic Methods, Ind. Eng. Chem. Res. 45(2006) 4389-4415. https://doi.org/10.1021/ie060370h.

[27] T. Lu, F. Chen, Multiwfn: a multifunctional wavefunction analyzer, J. Comput. Chem., 33(2012) 580-592. https://doi.org/10.1002/jcc.22885.

[28] J. Qi, Y. Qu, M. Zhou, Z. Su, X. Zhang, R. Wei, K. Xue, Y. Wang, 2023. Phase behavior and molecular insights on the separation of dimethyl carbonate and methanol azeotrope by extractive distillation using deep eutectic solvents. Sep. Purif. Technol. 305, 122489. https://doi.org/10.1016/j.seppur. 2022.122489.

[29] Y. Dai, X. Chu, Y. Jiao, Y. Li, P. Cui, Z. Zhu, Y. Wang, 2022. Molecular insights into azeotrope separation in the methyl tert-butyl ether production process using ChCl-based deep eutectic solvents, Chem. Eng. Sci. 264, 118179. https://doi.org/10.1016/j.ces. 2022.118179.

[30] C. M. Hsieh, S. I. Sandler, S.T. Lin, Improvements of COSMO-SAC for vapor-liquid and liquid-liquid equilibrium predictions. Fluid Phase Equilibr. 297(2010)90-97. https://doi.org/10.1016/j.fluid.2010.06.011.

[31] S. Wang, S. I. Sandler, Refinement of COSMO-SAC and the applications, Ind. Eng. Chem. Res. 47(2015)1-15. https://doi.org/10.1021/ie070465z.

[32] H. Zhang, B. Huo, M. Sun, R. Shan, P. Cui, J. Yang, Y. Wang, S. Zheng, 2022. The mechanism explosion of separating binary azeotropic system with intermediate-boiling-point solvent based on vapor‑liquid equilibrium experiment, quantum chemical calculation and molecular dynamics simulation, J. Chem. Thermodyn. 168, 106730. https://doi.org/10.1016/j.jct.2022.106730.

[33] Y. Shen, Q. Zhao, H. Li, X. Liu, Y. Wang, 2021. Design and optimization of reactive dividing-wall extractive distillation process for dimethyl carbonate synthesis based on quantum chemistry and molecular dynamics calculation. Sep. Purif. Technol. 273, 118978. https://doi.org/10.1016/j.seppur.2021.118978.

[34] M. J. Frisch, G. W. Trucks, H. B. Schlegel, Gaussian 09, Revision A.02. Gaussian, Inc.: Wallingford CT. 2009.

[35] W. Humphrey, A. Dalke, K. Schulten, VMD - Visual Molecular Dynamics, J. Molec. Graphics, 14(1996) 33-38. https://doi.org/10.1016/0263-7855(96)00018-5.

[36] W. Zhang, Z. Chen, Y. Shen, Molecular Mechanism and Extraction Performance Evaluation for Separation of Methanol and n-Hexane via Ionic Liquids as Extractant. ACS Sustainable Chem. Eng. 8(2020) 8700-8712. https://doi.org/10.1021/acssuschemeng.0c02234.

[37] T. Lu, Sobtop, Version1.0(dev3.2). http://sobereva.com/soft/Sobtop. 2024.

[38] M.J. Abraham, T. Murtola, R. Schulz, S. Páll, J.C. Smith, E. Lindahl, GROMACS: High performance molecular simulations through multi-level parallelism from laptops to supercomputers. SoftwareX. 1-2 (2015) 19-25. https://doi.org/10.1016/j.softx.2015. 06.001

[39] L. Martínez, R. Andrade, E.G. Birgin, PACKMOL: a package for building initial configurations for molecular dynamics simulations. Journal of Computational Chemistry. 30(2009), 2157-2164. https://doi.org/10.1002/jcc.21224

[40] M. Brehm, B. Kirchner, TRAVIS - a free analyzer and visualizer for monte carlo and molecular dynamics trajectories. J Chem Inf Model. 51(8)(2011) 2007-2023. https://doi.org/10.1186/1758-2946-4-S1-F1

[41] X. You,, J. Gu, C. Peng, W. Shen, Improved Design and Optimization for Separating Azeotropes with Heavy Component as Distillate through Energy-Saving Extractive Distillation by Varying Pressure, Ind. Eng. Chem. Res. 56(2017)9156-9166. https://doi.org/10.1021/acs.iecr.7b00687.

[42] Y. Fan, Q. Ye, H. Cen, Design and optimization of reactive distillation processes for synthesis of isopropanol based on self-heat recuperation technology. Chemical Engineering Research and Design, 147(2019) 171-186. https://doi.org/10.1016/j.cherd.2019.05.004.

[43] A. Yang, S. Sun, A. Eslamimanesh, Energy-saving investigation for diethyl carbonate synthesis through the reactive dividing wall column combining the vapor recompression heat

pump or different pressure thermally coupled technique. Energy. 172(2019) 320-332. https://doi.org/10.1016/j.energy.2019.01.126.

[44] B. Dai, H. Qi, S. Liu, Z. Zhong, H. Li, M. Song, M. Ma, Z. Sun, 2019. Environmental and economical analyses of transcritical CO_2 heat pump combined with direct dedicated mechanical subcooling (DMS) for space heating in China, Energy Conversion and Management. 198, 111317. https://doi.org/10.1016/j.enconman.2019.01.119.

[45] A. Amuel, U.S. Kennedy, EPA Office of Pollution Prevention and Toxics. New Chemicals Division (7403M). 1201 Pennsylvania Ave, NW. Washington, DC 20460

[46] R. F. Bader, M. T. Carroll, J. R. Cheeseman,, C. Chang, Properties of atoms in molecules: atomic volumes, J. Am. Chem. Soc. 109(1987)7968-7979. https://doi.org/10.1021/ja00260a006.

[47] J. S. Anthony, Natural bond orbitals and the nature of the hydrogen bond. The Journal of Physical Chemistry A. 121(2017)1531-1534. https://doi.org/10.1021/acs.jpca.6b12930.

[48] E. Arunan, G. R. Desiraju, R. A. Klein, J. Sadlej, S. Scheiner, I. Alkorta, Definition of the hydrogen bond (IUPAC Recommendations 2011). Pure and applied chemistry. 83(2011) 1637-1641. https://doi.org/10.1351/pac-rec-10-01-02.

[49] J. S. Murray, P. Politzer, Molecular electrostatic potentials and noncovalent interactions, WIREs Comput. Mol. Sci. 7 (6) (2017)1326. https://doi.org/10.1002/wcms.1326.

[50] T. Lu, Q. Chen, Revealing the nature of intermolecular interaction and configurational preference of the nonpolar molecular dimers $(H_2)2$, $(N_2)2$, and $(H_2)(N_2)$, J. Mol. Model. 19 (2022) 5387-5395. https://doi.org/10.1007/s00894-013-2034-2

[51] H. K. Hansen, P. Rasmussen, A. Fredenslund, M. Schiller, J. Gmehling, Vapor-Liquid Equilibria by UNIFAC Group Contribution.5. Revision and Extension. Ind. Eng. Chem. Res. 30 (10) (1991) 2352−2355. https://doi.org/10.1021/ie00058a017.

[52] Y. Dong, C. Dai, Z. Lei, Extractive distillation of methylal/methanol mixture using ethylene glycol as entrainer. Fluid Phase Equilibr. 462(2018)172-180. https://doi.org/10.1016/j.fluid.2018.01.038.

[53] Z. Lei, C. Dai, X. Liu, L. Xiao, B. Chen, Extension of the UNIFAC Model for Ionic Liquids. Ind. Eng. Chem. Res. 51 (37)(2012)12135−12144. https://doi.org/10.1021/ie301159v.

[54] Z. Lei, J. Zhang, Q. Li, B. Chen, E.C. Research, UNIFAC model for ionic liquids, Ind. Eng.

Chem. Res. 48(5)(2009) 2697-2704. https://doi.org/10.1021/ie801496e.

[55] Y. Dong, C. Dai, Z. Lei, Separation of the Methanol−Ethanol−Water Mixture Using Ionic Liquid. Ind. Eng. Chem. Res. 57(2018) 11167−11177. https://doi.org/10.1021/acs.iecr.8b01617.

[56] J.O. Valderrama, W.W. Sanga, J. A. Lazzús, Critical Properties, Normal Boiling Temperature, and Acentric Factor of Another 200 Ionic Liquids,Ind. Eng. Chem. Res. 47(2008)1318-1330. https://doi.org/10.1021/ie071055d.

[57] C. Sun, B. Peng, F. Xue, P. Cui, G. Li, Y. Wang, 2026. Mechanism research and process design for the separation of dimethyl carbonate and n-propanol by extractive distillation using ionic liquid. Journal of Environmental Management. 401, 129014. https://doi.org/10.1016/ j.jenvman.2026.129014

Supplementary Files

This is a list of supplementary files associated with this preprint. Click to download.

- SupplementaryMaterial.docx